



# Experimental investigations on the thermal conductivity characteristics of Beishan granitic rocks for China's HLW disposal



X.G. Zhao<sup>a,\*</sup>, J. Wang<sup>a</sup>, F. Chen<sup>a,b</sup>, P.F. Li<sup>a</sup>, L.K. Ma<sup>a</sup>, J.L. Xie<sup>a</sup>, Y.M. Liu<sup>a</sup>

<sup>a</sup> CNNC Key Laboratory on Geological Disposal of High-level Radioactive Waste, Beijing Research Institute of Uranium Geology, Beijing 100029, China

<sup>b</sup> School of Civil and Environmental Engineering, University of Science and Technology Beijing, Beijing 100083, China

## ARTICLE INFO

### Article history:

Received 28 December 2015

Received in revised form 26 April 2016

Accepted 18 June 2016

Available online 20 June 2016

### Keywords:

Thermal conductivity

Water saturation

Temperature

Axial stress

Beishan granite

Geological disposal

## ABSTRACT

Crystalline rocks are potential host rock types for the construction of high-level radioactive waste (HLW) repositories. A better understanding of thermal conductivity of rocks is essential to safe evaluation and engineering optimization of a HLW disposal system in the rock at depth. In the present study, experimental investigations on the thermal conductivity characteristics of 47 pairs of granitic rock specimens were conducted using the Transient Plane Source (TPS) method. The specimens were collected from borehole cores in the Beishan area, which is being considered as the most potential candidate area for China's HLW repository. To evaluate geological nature of the rocks, mineralogical compositions of the rocks were identified, and porosity of the specimens was measured. The thermal conductivities of the specimens under dry and water-saturated conditions were determined, and the effect of water saturation on the thermal conductivity was investigated. In addition, the influence of temperature and axial compression stress on the thermal conductivity of dry specimens was studied. The results revealed that the thermal conductivity of tested rocks was dependent on water saturation, temperature and compression stress. Based on the obtained data, some models considering porosity were established for describing the thermal conductivity characteristics of the tested rocks. Furthermore, when the rocks have a similar porosity, the quartz content dominates the thermal conductivity, and there exists an obvious increase of the thermal conductivity with increasing quartz content. The test results constitute the first systematic measurements on the Beishan granitic rocks and can further be used for the development of thermal models for predicting thermal response near the underground excavations for HLW disposal.

© 2016 Elsevier B.V. All rights reserved.

## 1. Introduction

Deep geological disposal has been the internationally accepted approach for the permanent disposal of high level radioactive waste (HLW) generated from nuclear power plants and other nuclear facilities. An HLW repository can be constructed in a host rock at a depth of several hundred meters below the ground surface. The design of HLW repositories often relies on a multi-barrier system, which typically consists of the natural geological barrier and an engineered barrier system. As the last defense to the biosphere, the natural geological barrier (i.e., the host rock) plays a critical role in ensuring the long-term safety of the HLW repositories. Because crystalline rocks such as granite and diorite have low permeability, high solidity, and good excavation stability, they have been considered as potential HLW repository formations in some countries (Hudson et al., 2011; Wang, 2014). Site selection for China's HLW repository started in 1985 (Wang, 2010). The efforts have been focused on potential HLW repository sites located within granite intrusions in mainland China. Since 1999, the Beijing Research

Institute of Uranium Geology (BRIUG) has performed site characterization studies in the Beishan area, China. So far, the Beishan area has been considered as the most potential candidate area for China's HLW repository.

Among all the engineering properties of crystalline rocks at a potential HLW repository site, the thermal conductivity is one of the most important parameters in design consideration because it has a direct impact on the evaluation of the necessary repository volume and the optimization of the repository layout (Sundberg and Hellström, 2009). For instance, in the Swedish KBS-3 concept for geological disposal of spent fuel, copper canisters with cast iron inserts containing the spent fuel are surrounded by bentonite for isolation and mechanical protection (Brantberger et al., 2006). The heat generated by the spent fuel will increase the temperature of all components of the repository. For the bentonite buffer outside the canisters, the peak temperature must not exceed 100 °C. This requirement implies that the canisters cannot be deposited arbitrarily close to each other. On the other hand, unnecessarily large distances between the canisters will mean inefficient and costly use of the repository rock volume (Hökmark et al., 2009). To fulfill the temperature requirement, the rocks with low thermal conductivities will

\* Corresponding author.

E-mail address: [xingguang100@126.com](mailto:xingguang100@126.com) (X.G. Zhao).

lead to a larger distance between canisters than for a case with high thermal conductivities. This is because the rocks with low thermal conductivities will give rise to higher temperatures in the bentonite (Sundberg et al., 2008). Hence, to design and construct repositories successfully, it is essential to perform an accurate assessment of the thermal conductivity characteristics of the host rock.

Over the past few decades, various experimental approaches have been employed to measure the thermal conductivity of rocks. The results indicate that the thermal conductivity of rocks is closely associated with mineral composition, porosity, texture, and density, etc. (Birch and Clark, 1940; Clauser and Huenges, 1995; Hartmann et al., 2005; Özkahraman et al., 2004; Pasquale et al., 2015; Ray et al., 2007; Sundberg et al., 2009). For crystalline rocks with relatively homogeneous texture and low porosity, the mineral composition dominates the thermal conductivity. In volcanic and sedimentary rocks, the high variability of porosity in these rocks is a major factor controlling the thermal conductivity (Clauser and Huenges, 1995; Özkahraman et al., 2004). For example, increasing porosity, which acts as barrier to the flow of heat, often results in both lower P-wave velocity and lower thermal conductivity values (Özkahraman et al., 2004). For a given rock, water content and temperature have an influence on its thermal conductivity. Generally, the thermal conductivity of the rock increases and decreases with increasing water content (Cho and Kwon, 2010; Cho et al., 2009) and temperature (Abdulagatova et al., 2009; Birch and Clark, 1940; Heuze, 1983; Miao et al., 2014; Mottaghy et al., 2008; Vosteen and Schellschmidt, 2003), respectively. Moreover, the effect of water saturation on the thermal conductivity of rocks shows a generally increasing trend with increasing porosity (Nagaraju and Roy, 2014). Given that the thermal conductivity of surrounding rocks around the excavations will be changed by the excavation-induced stress, some researchers studied the influence of pressure on the thermal conductivity of rocks (Abdulagatova et al., 2010; Abdulagatova et al., 2009; Demirci et al., 2004; Görgülü et al., 2008; Sibbitt, 1976; Walsh and Decker, 1966; Zimmerman, 1989). One of the main findings achieved from these investigations shows that the thermal conductivity

varies with the pressure exerted on the rock. With increasing applied pressure, the thermal conductivity starts to increase and subsequently the increase rate tends to be a constant value due to gradual closure of cracks and pores within the rock (Görgülü et al., 2008; Walsh and Decker, 1966).

While the above-mentioned studies provide meaningful insight into the thermal conductivity of various rocks, the thermal conductivity characteristics of low-porosity crystalline rocks subjected to different external factors such as water saturation, temperature and compression stress have not been fully understood. On the other hand, the information on the thermal conductivity of rocks in a potential HLW repository site must be known with sufficient confidence to provide necessary input conditions for its long-term safety assessment, which is one of the motivations for this study. In this work, experimental investigations on the thermal conductivity of the Beishan granitic rocks are conducted using the Transient Plane Source (TPS) method. In the following discussion, rock sampling and basic physical properties of the rock specimens are introduced first. Testing facilities and procedures are then described. Subsequently, the water saturation, temperature and compression stress dependent thermal conductivity characteristics of the tested rocks are evaluated comprehensively, and finally some insights are obtained.

## 2. Rock sampling and preparation

The Beishan area is situated in Gansu Province of northwestern China (see Fig. 1). After a long geological evolution and weathering process, the topography of this area is characterized by a flat Gobi and small gentle rolling hills with elevations ranging between 1400 and 2000 m above the sea level. The crust in this area possesses a blocky structure with many granite intrusions (see Fig. 2). Other surrounding rocks include mainly metamorphic and sedimentary rocks, as well as Quaternary cover. Rock sampling was carried out in the Jijicao and Xinchang rock blocks, which are currently considered as two of the key investigation sub-areas during site selection and characterization.

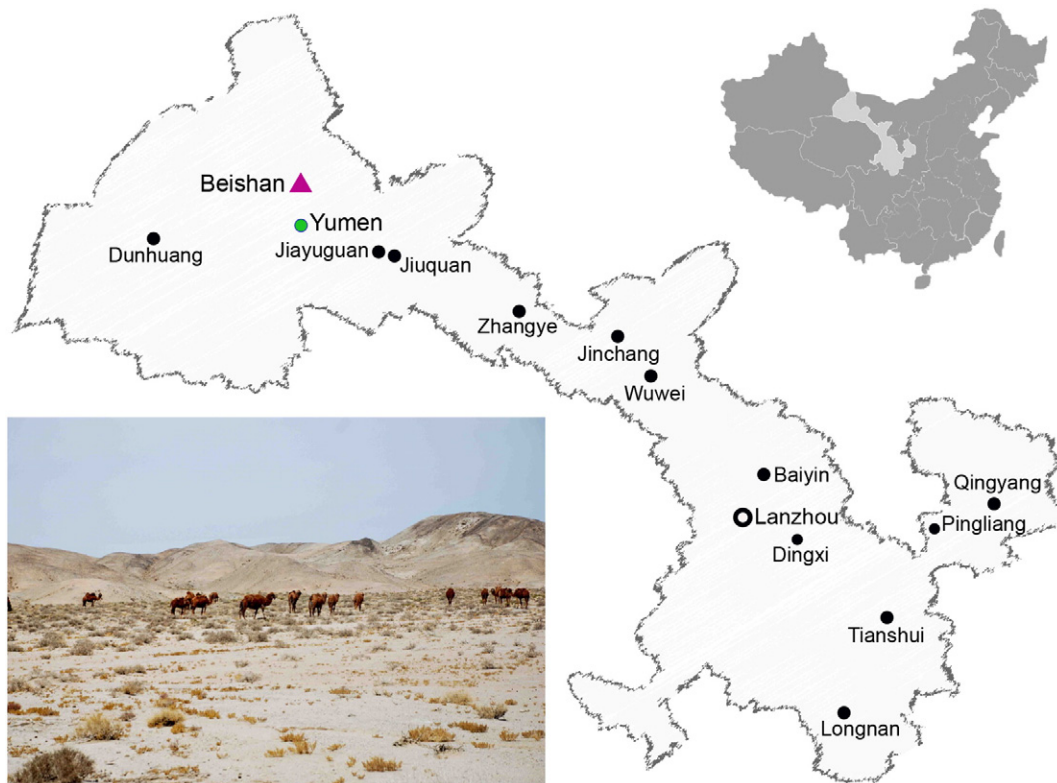


Fig. 1. Geographical location of the Beishan area and a photo showing its typical topography.

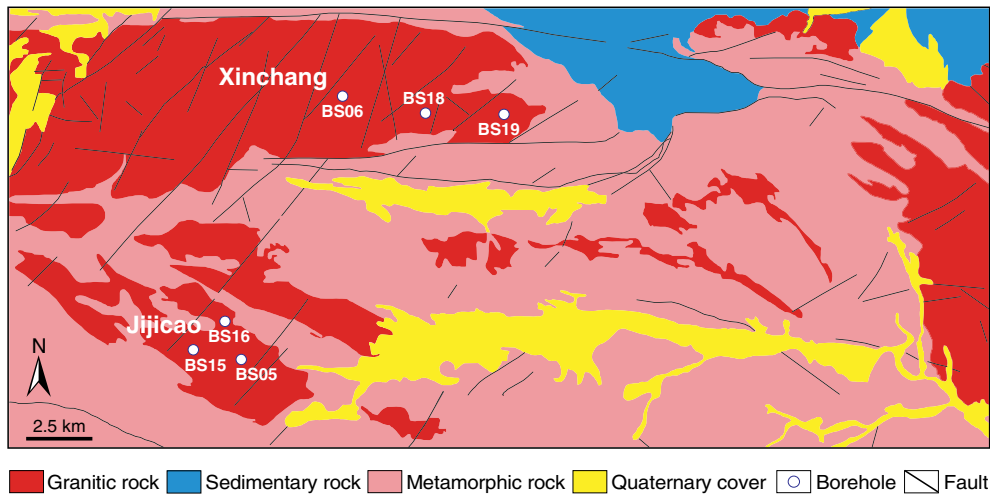


Fig. 2. Rock sampling from six boreholes in the Jijicao and Xinchang sub-areas for thermal conductivity measurements.

Intact drill cores with a diameter of approximately 63 mm were taken from six sub-vertical boreholes (i.e., boreholes BS05, BS06, BS15, BS16, BS18 and BS19) in these two sub-areas. The borehole locations are presented in Fig. 2.

Field observations indicated that the collected granitic rocks were relatively isotropic in texture and mineralogical composition. To evaluate the geological nature of the rocks, a series of thin sections were prepared and then exposed to cross-polarized light under an optical microscope to identify the dominant minerals in the rocks. The percentages of the dominant minerals were determined by point counting on thin sections. For each thin section approximately 500 points covering phenocrysts and groundmass were counted. According to the quartz-alkali feldspar-plagioclase (QAP) diagram (Streckeisen, 1976), the rocks can further be classified. It can be observed from Fig. 3 that the rocks contain mainly a moderate to low amount of quartz and alkali feldspar, and a moderate to high amount of plagioclase. This means that the collected rocks dominantly range from granodiorite to monzogranite. For grain size characteristics, the rocks are from fine grained to, medium to coarse grained. An overview of the basic information of the rocks is listed in Table 1. Based on the borehole no. and sampling depth, these rocks have been divided into eight groups.

A total of 47 pairs of rock specimens, 50 mm in diameter, were prepared from the drill cores with a length to diameter ratio of approximately 0.5. In particular, specimen ends were polished using a

grinding machine until the flatness and roughness of the ends are less than 10  $\mu\text{m}$  and 3  $\mu\text{m}$ , respectively. The flat and polished specimen end surfaces minimize the thermal contact resistance during thermal conductivity measurement. A minimum of ten specimens for each rock group were prepared.

### 3. Test methodology

#### 3.1. An introduction to the used TPS method

In the fields of geology and geophysics, laboratory approaches to measuring soil and rock thermal conductivity can mainly be divided into two groups: steady state and transient state. In this work, the Transient Plane Source (TPS) method (Gustafsson, 1991; Log and Gustafsson, 1995) was utilized to measure the thermal conductivity of the specimens. As one of the transient measurement methods, the TPS technique is based on the use of a transiently heated plane sensor (i.e., Hot Disk sensor) and a Hot Disk Thermal Constants Analyser (see Fig. 4a). The used Hot Disk TPS2500S system can measure thermal conductivity of materials ranging from 0.01 to 400 W/mK. The Hot Disk sensor consists of a continuous double spiral, which is etched out of a thin nickel foil (Fig. 4e). This spiral is sandwiched between two sheets of electrical insulation materials made of Kapton. The sensor acts both as a heat source for increasing the temperature of the specimens and as a dynamic temperature sensor for recording the temperature increase. During the measurement, the temperature in the sensor rises and heat starts to flow to the specimens. The temperature rise in the sensor provides an indicator of the thermal properties of the specimens. If the specimens have good thermal conducting properties, the heat will be transported rapidly inside the specimens. On the contrary, if the specimens have good thermal insulation properties, the sensor temperature will rise faster and the heat will not be transported as much as in the test of the good thermal conducting specimens. Compared with steady state measurement methods such as the divided bar (Beck and Beck, 1958; Birch, 1950; Sass et al., 1971) and the guarded hot plate (Abdulagatova et al., 2009; Alishaev et al., 2012), one of significant advantages of the TPS technique is that the thermal conductivity of materials can be measured more quickly, typically from several to tens of seconds. Hence, a long wait for thermal gradients to equilibrate is not required and the moisture migration in response to temperature gradients was minimized (Jackson and Taylor, 1986). On the other hand, unlike some transient methods such as thermal needle probes (Barry-Macaulay et al., 2013; Von Herzen and Maxwell, 1959), which are commonly used for soils and soft rocks, the TPS method can be

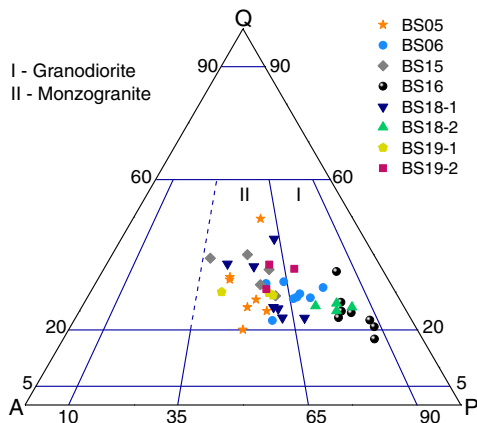
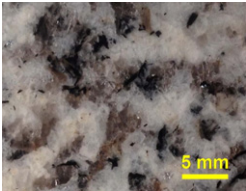
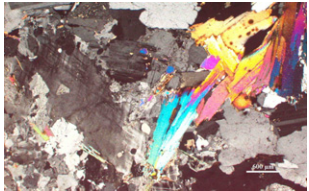
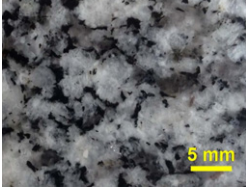
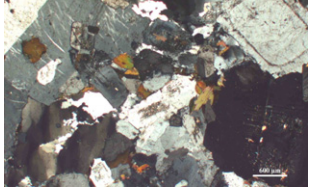
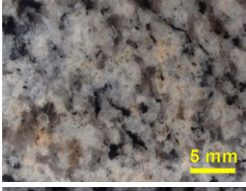
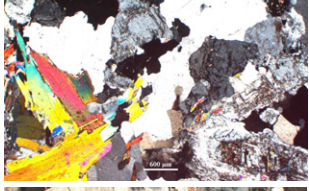
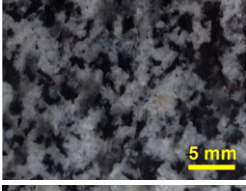

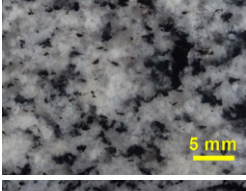
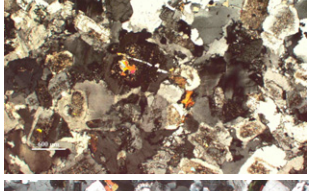
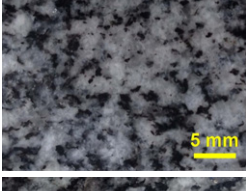
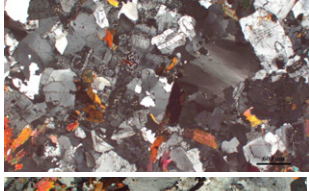
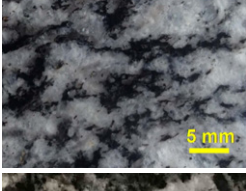
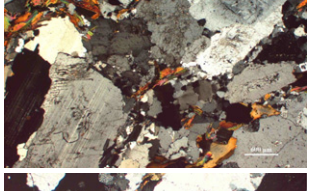
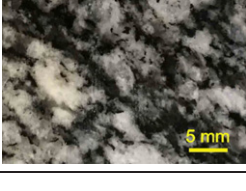
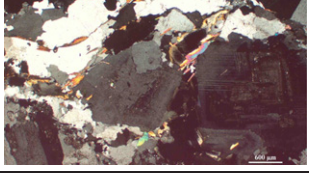


Fig. 3. QAP classification of the eight rock groups based on modal analysis.

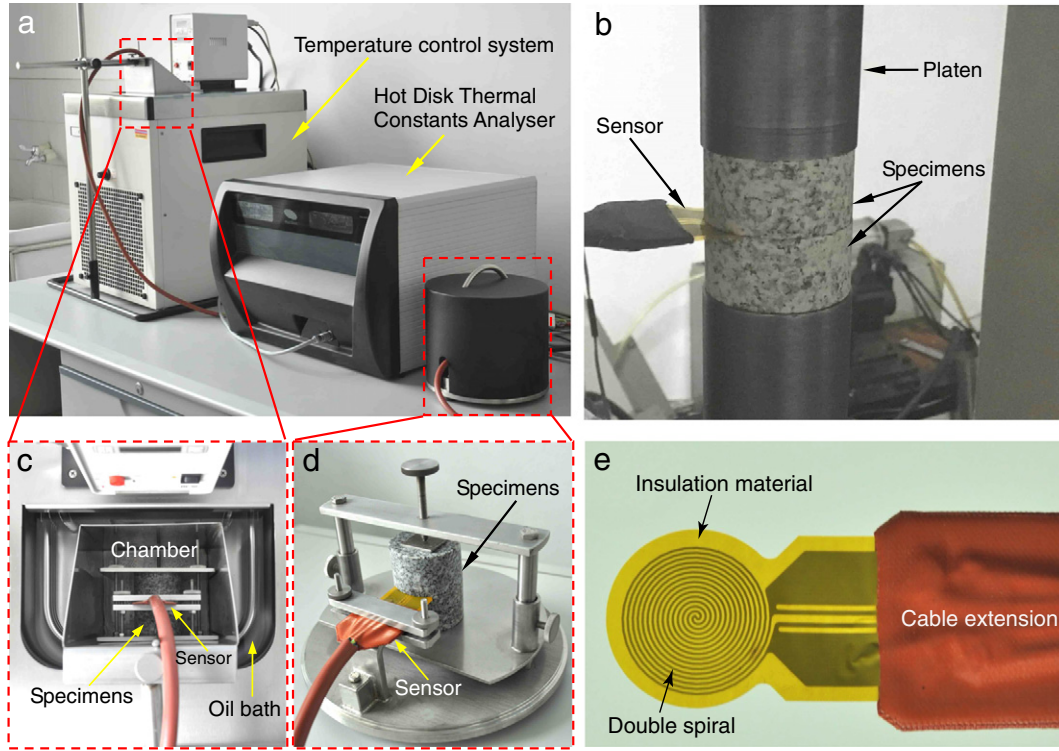


**Table 1**  
Basic information and geological description of the tested rocks.

Rock type and group	Basic information	Mineral composition	Naked eye observation	Photomicrograph of a thin section
Monzogranite (BS05)	Location: Jijicao Borehole no.: BS05 Sampling depth: 5–7 m Number of specimen pairs: 7 Grain size: medium	Plagioclase: $33.7\% \pm 5.8\%$ ; K-feldspar: $30.7\% \pm 6.1\%$ ; Quartz: $28.6\% \pm 8.0\%$ ; Biotite: $7.1\% \pm 4.8\%$ (Number of thin sections: 8)		
Granodiorite (BS06)	Location: Xinchang Borehole no.: BS06 Sampling depth: 434–435 m Number of specimen pairs: 5 Grain size: medium	Plagioclase: $44.6\% \pm 4.6\%$ ; K-feldspar: $22.6\% \pm 4.5\%$ ; Quartz: $27.4\% \pm 3.1\%$ ; Biotite: $5.0\% \pm 1.3\%$ (Number of thin sections: 8)		
Monzogranite (BS15)	Location: Jijicao Borehole no.: BS15 Sampling depth: 467–474 m Number of specimen pairs: 7 Grain size: fine to medium	Plagioclase: $31.4\% \pm 6.9\%$ ; K-feldspar: $27.6\% \pm 5.3\%$ ; Quartz: $32.0\% \pm 4.3\%$ ; Biotite: $9.0\% \pm 3.9\%$ ; (Number of thin sections: 5)		
Granodiorite (BS16)	Location: Jijicao Borehole no.: BS16 Sampling depth: 561–563 m Number of specimen pairs: 5 Grain size: fine to medium	Plagioclase: $57.2\% \pm 7.2\%$ ; K-feldspar: $11.1\% \pm 2.0\%$ ; Quartz: $22.1\% \pm 4.7\%$ ; Biotite: $8.4\% \pm 2.2\%$ (Number of thin sections: 8)		
Monzogranite (BS18-1)	Location: Xinchang Borehole no.: BS18 Sampling depth: 445–459 m Number of specimen pairs: 8 Grain size: fine	Plagioclase: $37.4\% \pm 8.3\%$ ; K-feldspar: $25.7\% \pm 4.1\%$ ; Quartz: $28.3\% \pm 8.1\%$ ; Biotite: $4.7\% \pm 1.8\%$ (Number of thin sections: 7)		
Granodiorite (BS18-2)	Location: Xinchang Borehole no.: BS18 Sampling depth: 489–505 m Number of specimen pairs: 5 Grain size: fine	Plagioclase: $52.9\% \pm 3.6\%$ ; K-feldspar: $14.4\% \pm 3.0\%$ ; Quartz: $23.7\% \pm 1.4\%$ ; Biotite: $9.0\% \pm 2.7\%$ (Number of thin sections: 4)		
Monzogranite (BS19-1)	Location: Xinchang Borehole no.: BS19 Sampling depth: 499–500 m Number of specimen pairs: 6 Grain size: coarse	Plagioclase: $34.4\% \pm 6.2\%$ ; K-feldspar: $29.5\% \pm 5.7\%$ ; Quartz: $27.0\% \pm 0.8\%$ ; Biotite: $5.4\% \pm 1.1\%$ (Number of thin sections: 3)		
Monzogranite (BS19-2)	Location: Xinchang Borehole no.: BS19 Sampling depth: 512–514 m Number of specimen pairs: 4 Grain size: coarse	Plagioclase: $34.8\% \pm 2.1\%$ ; K-feldspar: $21.7\% \pm 5.7\%$ ; Quartz: $30.0\% \pm 2.5\%$ ; Biotite: $8.1\% \pm 3.1\%$ (Number of thin sections: 3)		

easy to apply to hard geomaterials such as crystalline rocks. It should be noted that the TPS method measures the thermal conductivity in a contact manner, which is different from non-contact optical scanning

measurements (Popov et al., 1999; Popov et al., 2003). Hence, the thermal resistance between the specimen ends and the sensor exists (see Section 3.2). So far, the TPS technology has been widely used to



**Fig. 4.** The Hot Disk TPS2500S system (a) used to measure the thermal conductivity of specimens under room temperature (d), high temperature (c), and uniaxial compression (b) conditions. A Hot Disk sensor showing its key components (e).

determine the thermal properties of different materials (Lagüela et al., 2015; Solórzano et al., 2008; Urquhart and Bauer, 2015; Xu et al., 2014; Yang et al., 2012).

### 3.2. Theory of the TPS technique

To theoretically describe how the TPS method behaves, the thermal conductivity equation can be solved assuming that the Hot Disk sensor consists of a certain number of concentric ring heat sources located in an infinitely large sample (Hot Disk, 2007). A constant electric power supplied to the sensor results in an increase in temperature which is directly related to the variation in the sensor resistance ( $R(t)$ ) by the equation:

$$R(t) = R_0 \left( 1 + \alpha \overline{\Delta T(\tau)} \right) \quad (1)$$

where  $R_0$  is the nickel electrical resistance in the beginning of the recording,  $\alpha$  is the temperature coefficient of resistance of the nickel foil, and  $\overline{\Delta T(\tau)}$  is the mean value of temperature rise in the sensor due to a constant current pulse given by:

$$\overline{\Delta T(\tau)} = P_0 \left( \pi^{3/2} a k \right)^{-1} D(\tau) \quad (2)$$

where  $P_0$  is the total output of power from the sensor,  $a$  is the sensor radius,  $k$  is the thermal conductivity of the sample that is being tested and  $D(\tau)$  is a dimensionless time dependent function with:

$$\tau = (t/\theta)^{1/2}; \quad \theta = a^2/d \quad (3)$$

where  $t$  is the time measured from the start of the transient recording,  $\theta$  is the characteristic time, which depends both on parameters of the sensor and the sample, and  $d$  is the thermal diffusivity of the sample.

According to Eq. (2), and  $\overline{\Delta T(\tau)}$  and  $D(\tau)$  plotted as a function of  $\tau$  provides a linear relationship with a slope that is a function of  $P_0$ ,  $a$ , and  $k$ . Thermal conductivity  $k$  can be obtained by fitting the experimental data to the straight line given by Eq. (2); thermal diffusivity  $d$  is calculated from Eq. (3) taking into account the  $\tau$  value determined in the previous fit.

As mentioned above, the solution of the thermal conductivity equation is based on the assumption that the Hot Disk sensor is located in an infinite material in perfect contact with the sensor surface. This means that the heat flow generated from each measurement must not reach the outside boundaries of the specimen (Hot Disk, 2007). Meanwhile, a careful preparation of specimen ends is required to minimize thermal contact resistance. An estimation of how far the heat flow has proceeded in the specimen during a recording is the probing depth  $\Delta_p$ , which is defined as (Hot Disk, 2007):

$$\Delta_p = 2\sqrt{dt} \quad (4)$$

To determine the thermal conductivity with good accuracy, the shortest distance from any part of the sensor to the nearest outside boundary of the sample should be larger than  $\Delta_p$ . In our experiments, the used Hot Disk sensor has a radius of 6.403 mm. The shortest distance is about 19 mm, and the probing depth is approximately 10 mm. For this probing depth value, we can consider that we are conducting a bulk measurement.

### 3.3. Test procedures

#### 3.3.1. Tests on specimens under saturated and dry conditions

Firstly, the specimens were immersed by deionized water in a vacuum for a period of 96 h. The specimens were then taken from the vacuum and the water droplets on the surfaces were wiped dry, care being taken to ensure that no rock grains or fragments were lost. The mass of the water-saturated specimens ( $M_{sat}$ ) was measured using a

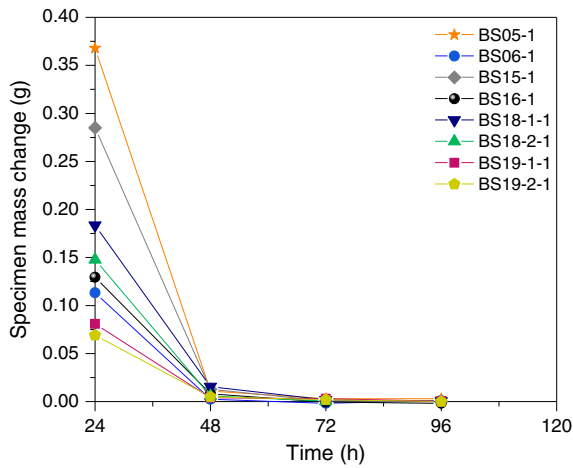


Fig. 5. Typical curves showing the mass changes of several specimens during saturation.

high precision balance (to 0.0001 g). Our tests revealed that the mass of the specimens could be approximately constant under vacuum within 72 h (see Fig. 5), indicating that the specimens were saturated with water. Subsequently, the Hot Disk sensor was horizontally placed between the two saturated specimen pieces with the double spiral centered and totally covered, and the two specimen pieces were firmly clamped together to ensure that there was no air gap between the sensor and the specimen end surfaces, as presented in Fig. 4d. In order to remain water saturation, the saturated specimens and the sensor were kept in a plastic bag during thermal conductivity measurement (Adl-Zarrabi, 2004). After the test, the used water-saturated specimens were suffered from dehydration treatment in a thermostatic drying oven at 105 °C for a period of 24 h and subsequently cooled in a desiccator to measure the thermal conductivity under a dry condition. Meanwhile, the mass of the dry specimens ( $M_{dry}$ ) was measured, and the porosity ( $n$ ) of the specimens was calculated using the equations

$$n = \frac{100V_p}{V} \% \quad (5)$$

$$V_p = \frac{M_{sat} - M_{dry}}{\rho_w} \quad (6)$$

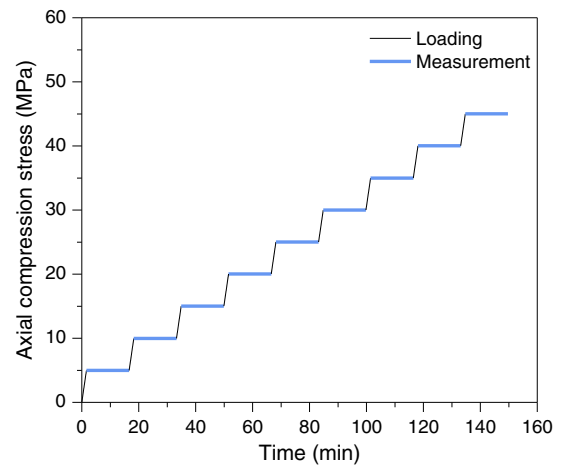


Fig. 7. The designed stress path in the thermal conductivity measurement.

where  $V$  is the bulk rock volume,  $V_p$  is the pore volume, and  $\rho_w$  is the density of water. For each pair of specimens saturated or dried, measurements on the thermal conductivity were carried out at room temperature ( $25 \pm 1$  °C).

### 3.3.2. Tests on specimens under increasing temperature

To investigate the effect of temperature on the thermal conductivity of the tested rocks, measurements were performed on dry specimens from 40 °C to 150 °C based on the requirements of the used test equipment. Compared with measurements at room temperature, the experiments under high temperature are time consuming due to a slow stepwise heating process by using a constant temperature oil bath and a temperature control system, as shown in Fig. 4c. The thermal conductivity measurement can only be conducted until the two specimen pieces in the chamber with a specimen holder within the oil bath have reached thermal equilibrium and kept a target temperature value. During thermal equilibrium of the oil bath, the Hot Disk sensor monitors continuously the temperature variation of the specimens. For our tests, the thermal conductivity of the specimens was measured when the recorded temperature variation of the specimens is less than 0.04 °C. In general, 32 h were needed to complete one test. A typical temperature-time history during the test is presented in Fig. 6. It should

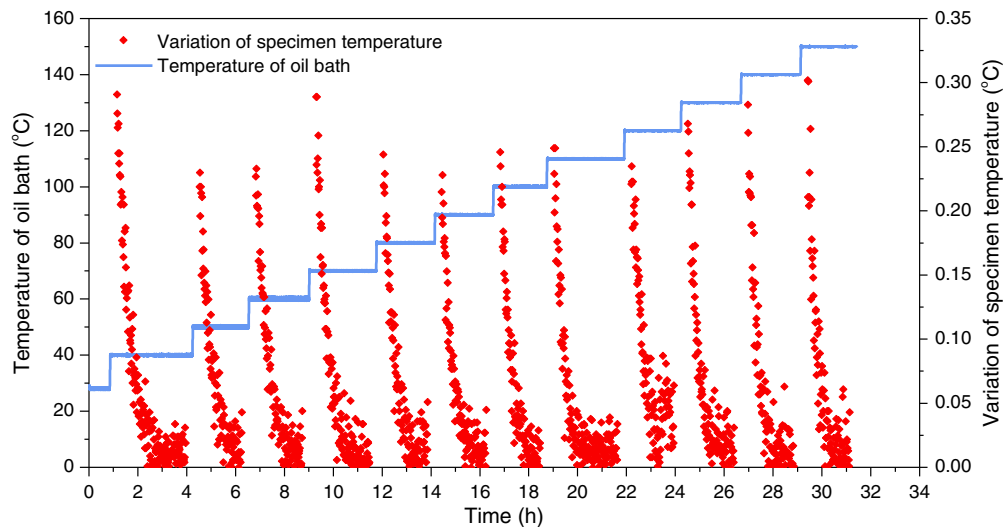


Fig. 6. A typical temperature-time history showing the variation of the oil bath temperature with time, and the evolution of specimen temperature variation during the thermal conductivity measurement on a pair of specimens.



**Table 2**

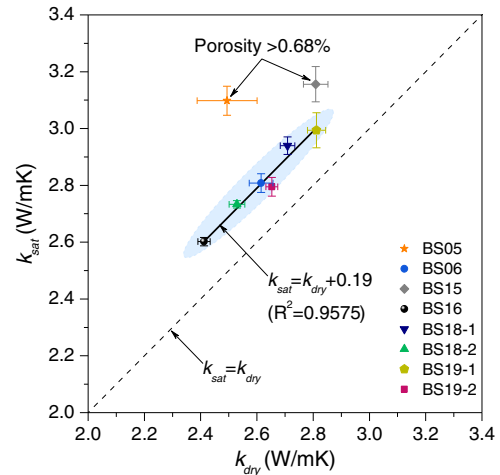
Porosity, thermal conductivity and effect of water saturation for 40 pairs of Beishan granitic rock specimens under dry and water-saturated conditions.

Rock type and group	Specimen pair no.	Density (kg/m <sup>3</sup> )	Porosity (%)	Thermal conductivity (W/mK)		Effect of water saturation S (%)
				$k_{dry}$	$k_{sat}$	
Monzodiorite (BS05)	BS05-01	2602	1.35	2.572	3.087	20.02
	BS05-02	2631	1.37	2.633	3.115	18.31
	BS05-03	2597	1.35	2.426	3.033	25.02
	BS05-04	2583	1.38	2.354	3.049	29.52
	BS05-05	2606	1.40	2.548	3.140	23.23
	BS05-06	2600	1.38	2.431	3.163	30.11
	Mean	2603	1.37	2.494	3.098	24.37
Granodiorite (BS06)	BS06-01	2640	0.46	2.669	2.769	3.75
	BS06-02	2633	0.54	2.621	2.794	6.60
	BS06-03	2630	0.46	2.568	2.827	10.09
	BS06-04	2636	0.38	2.600	2.843	9.35
	Mean	2635	0.46	2.615	2.808	7.44
Monzodiorite (BS15)	BS15-01	2616	0.82	2.765	3.107	12.37
	BS15-02	2618	0.77	2.853	3.190	11.81
	BS15-03	2618	0.68	2.873	3.136	9.15
	BS15-04	2608	0.71	2.800	3.263	16.54
	BS15-05	2601	0.62	2.782	3.142	12.94
	BS15-06	2604	0.48	2.782	3.095	11.25
	Mean	2611	0.68	2.809	3.156	12.34
Granodiorite (BS16)	BS16-01	2674	0.42	2.383	2.604	9.27
	BS16-02	2681	0.44	2.427	2.620	7.95
	BS16-03	2689	0.45	2.430	2.584	6.34
	BS16-04	2682	0.35	2.407	2.599	7.98
	Mean	2682	0.42	2.412	2.602	7.89
Monzodiorite (BS18-1)	BS18-1-01	2636	0.62	2.696	2.922	8.38
	BS18-1-02	2633	0.67	2.722	2.957	8.63
	BS18-1-03	2630	0.68	2.736	2.960	8.19
	BS18-1-04	2633	0.40	2.664	2.883	8.22
	BS18-1-05	2633	0.41	2.730	2.956	8.28
	BS18-1-06	2636	0.42	2.692	2.928	8.77
	BS18-1-07	2657	0.43	2.724	2.972	9.10
	Mean	2637	0.52	2.709	2.940	8.51
Granodiorite (BS18-2)	BS18-2-01	2645	0.58	2.514	2.742	9.07
	BS18-2-02	2652	0.52	2.556	2.732	6.89
	BS18-2-03	2655	0.32	2.548	2.743	7.65
	BS18-2-04	2655	0.40	2.497	2.715	8.73
	Mean	2652	0.46	2.529	2.733	8.08
Monzodiorite (BS19-1)	BS19-01	2660	0.42	2.680	2.774	3.51
	BS19-02	2661	0.42	2.663	2.799	5.11
	BS19-03	2660	0.42	2.606	2.795	7.25
	BS19-04	2660	0.42	2.634	2.779	5.50
	BS19-05	2654	0.42	2.682	2.827	5.41
	Mean	2659	0.42	2.653	2.795	5.36
Monzodiorite (BS19-2)	BS19-01	2655	0.41	2.792	2.988	7.02
	BS19-02	2654	0.37	2.845	3.020	6.15
	BS19-03	2648	0.40	2.876	3.017	4.90
	BS19-04	2649	0.43	2.736	2.950	7.82
	Mean	2652	0.40	2.812	2.994	6.47

be noted that the water-saturated specimens were not adopted in this test because little was known about how the gradual heating and the thermal equilibrium processes would affect the water content of the specimens, leading to difficulties in evaluating the relationship between the thermal conductivity and the water saturation degree of the specimens quantitatively.

### 3.3.3. Tests on specimens under uniaxial compression

The uniaxial compression tests on dry specimens were conducted using a hydraulic servo-controlled compression machine. For each test, two specimen pieces with the Hot Disk sensor were contained between steel platens machined to match their end surfaces, as shown in Fig. 4b. The interfaces between the specimens and the steel platens were daubed with a thin layer of lubricant to reduce the end effect of the platens during loading. When the experimental setup was completed, axial-load control was used with a loading rate of 100 N/s and the axial load was increased with an increment



**Fig. 8.** Comparison of the average thermal conductivity values measured under dry ( $k_{dry}$ ) and water-saturated ( $k_{sat}$ ) conditions for the eight rock groups. The shaded zone covers the rock groups with an average porosity range between 0.40 and 0.52. Error bars indicate the standard deviation of the thermal conductivity.

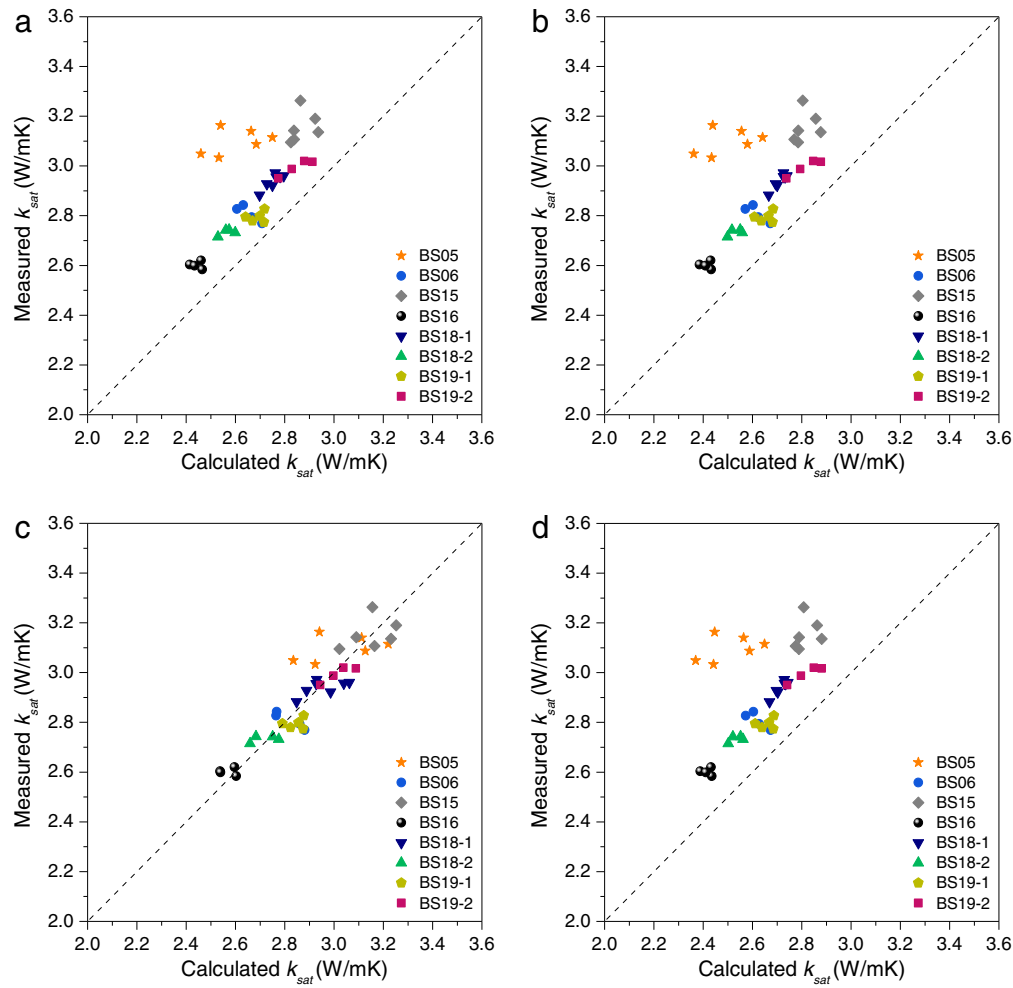
of 5 MPa. The thermal conductivity measurement was performed at each incremental stress level. After each measurement, the load was maintained constant for a period of about 15 min to avoid residual temperature drifts on the specimens. Based on the in-situ stress measurement results obtained from the Beishan area (Zhao et al., 2013), the maximum axial compression stress applied to the specimens was set to be 45 MPa to approximately simulate the excavation-induced stress near the vertical HLW disposal element boundary at a depth of 600 m. The axial stress applied to the specimens was recorded automatically, and the used stress path throughout the course of testing is presented in Fig. 7. The experiments were conducted at room temperature.

According to previous experimental results (Zhao et al., 2015a; Zhao et al., 2015b), the identified crack initiation stresses of cylindrical specimens of Beishan granitic rocks under uniaxial compression using the cumulative AE hit (CAEH) method range from 45.3 to 109.1 MPa, which are larger than the maximum compression stress adopted in the present study. Hence, the stress-induced rock damage might not occur in the tested specimens during loading. It should be mentioned that in the process of loading, the friction may occur at the interfaces between the specimen ends and the sensor. Due to limitation of the TPS measurement technique, the utilized test method does not consider the potential influence of interface friction effect on the experimental results. To reduce or eliminate the friction effect, further efforts are needed to produce innovative design for the test equipment. Although not perfect, the developed test system provides a feasible means for us to gain insight into thermal conductivity behaviors of rocks under compression.

## 4. Test results

### 4.1. Influence of water saturation on the thermal conductivity

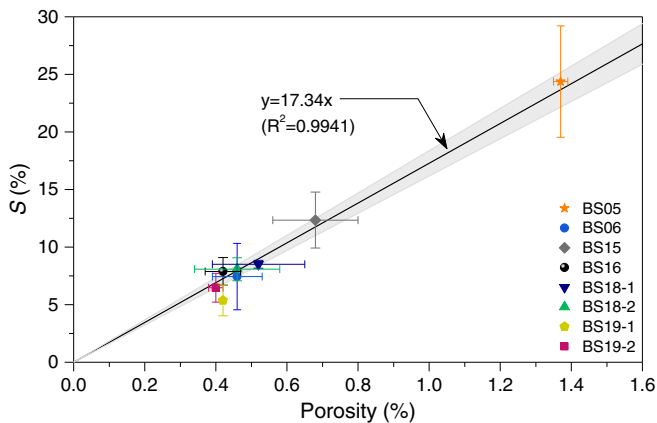
Thermal conductivity measurements were carried out on the 40 pairs of specimens both in dry and water-saturated conditions, and the results are listed in Table 2. A statistical analysis shows that for the eight rock groups under dry or saturated state, the standard deviation (SD) and coefficient of variation (CoV) of the thermal conductivity are all less than 0.06 W/mK and 4%, respectively, indicating that the results between specimens in each rock group have a good consistency. For all rock groups, the average thermal conductivity values in the dry state ( $k_{dry}$ ) range between 2.412 and 2.812 W/mK. The values under water-saturated condition ( $k_{sat}$ ) for the same set of specimens range from



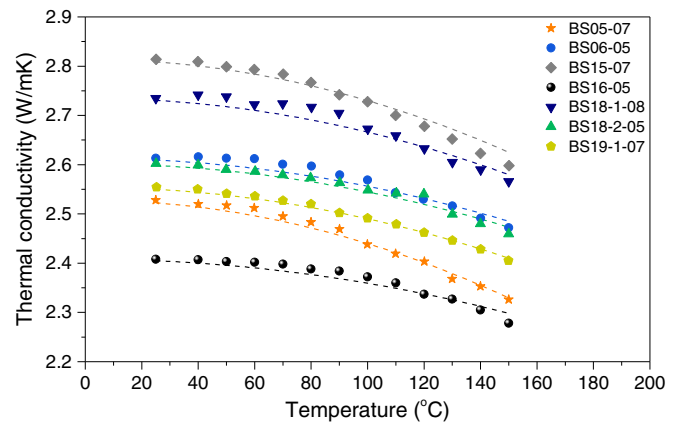
**Fig. 9.** Actual test data and calculated thermal conductivities of Beishan granitic rock specimens under water-saturated condition using four mixing models: arithmetic mean (a), geometric mean (b), Hashin-Shtrikman mean (c) and effective-medium mean.

2.602 to 3.156 W/mK. It is seen from Table 2 that the tested rocks have an average porosity range from 0.40% to 1.37%. When the dry specimens were saturated with water, water with a higher thermal conductivity (0.604 W/mK) replaced the air with a lower thermal conductivity (0.025 W/mK) in the void of the rocks, leading to an increase of the thermal conductivity. For our data set, the mean thermal conductivity values

of the saturated specimens in different rocks groups range from 6.5% to 24.2% higher than those of dry ones. As presented in Fig. 8, for the rock groups (i.e., BS06, BS16, BS18-1, BS18-2, BS19-1 and BS19-2) with an average porosity range between 0.40% and 0.52%, the influence of water saturation on the thermal conductivity of the rocks is relatively small, and  $k_{sat}$  increases with increasing  $k_{dry}$  in an approximately linear



**Fig. 10.** Variation of the effect of water saturation on thermal conductivity ( $S$ ) with porosity of the eight rock groups. The shaded zone represents the 95% confidence limit for the linear regression.



**Fig. 11.** Variation of thermal conductivity of seven pairs of specimens in different rock groups with increasing temperature up to 150 °C and their best fits.



behavior. However, with further increase of rock porosity, the approximately linear relationship between  $k_{dry}$  and  $k_{sat}$  is not valid anymore. For example, the rock groups BS05 and BS15 with average porosity values greater than or equal to 0.68% exhibit higher thermal conductivity in the water-saturated state relative to the dry state.

To evaluate the thermal conductivity of rocks, various mixing models such as the geometric mean (Lichtenecker, 1924), the arithmetic mean (Voigt, 1928), the Hashin–Shtrikman mean (Hashin and Shtrikman, 1962), and the effective-medium mean (Bruggeman, 1935; Clauser, 2009) have been proposed. Comprehensive overviews and case studies on such mixing models can be found in (Abdulagatova et al., 2009; Clauser, 2009; Fuchs et al., 2013; Hartmann, 2005; Ray et al., 2015). Based on the experimental data (see Table 2) in combination with the methodology used by Fuchs et al. (2013), the above-mentioned mixing models were used to predict the thermal conductivity values of the tested rocks in the water-saturated state. Fig. 9 shows the comparison between measured and calculated thermal conductivities for the four different models. It can be observed from Fig. 9a, b, and d that the geometric mean, the arithmetic mean, and the effective-medium mean yield similar prediction results and consistently underestimate the thermal conductivity of the eight rock groups, especially for the groups with relatively high porosity values (e.g., groups BS05 and BS15). The Hashin–Shtrikman mean shows a reasonably good fit for all rock groups, as shown in Fig. 9c. The analysis results are basically in line with observations reported by Fuchs et al. (2013) because most of the evaluated mixing models used in their analysis also underestimate the thermal conductivity of the rocks. However, the geometric mean model was rated as the best fit to their data set. It should be noted that the rocks used in their analysis covered different rock types with a large range in porosity, from almost zero to about 30%. In addition, the measured thermal conductivity values of these rocks spans the interval between 1.0 and 6.5 W/mK. The present investigations focused mainly on the granitic rocks with low porosities and a narrow thermal conductivity range. Hence, the large difference of rock properties may result in uncertainties between analysis results obtained from various mixing models. More work is required to explain this discrepancy.

Nagaraju and Roy (2014) defined the effect of water saturation on thermal conductivity ( $S$ ) as a function of porosity of rocks, and  $S$  is expressed by

$$S = \frac{k_{sat} - k_{dry}}{k_{dry}} \quad (7)$$

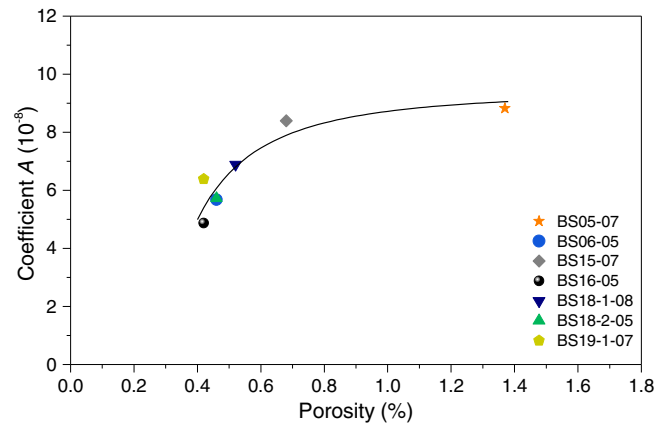
According to the measurement results listed in Table 2, we established the relationship between  $S$  and the porosity of the rocks, as presented in Fig. 10. Analysis of Fig. 10 reveals that the effect of water saturation on thermal conductivity of rocks presents an increasing trend with an increase of porosity. A linear form expression can fit the data reasonably well while ensuring that the line passes through the origin.

#### 4.2. Influence of temperature on the thermal conductivity

Fig. 11 presents the variation of thermal conductivity of seven pairs of specimens in different rock groups with temperature from 40 °C

**Table 3**  
Fit coefficient  $A$  for thermal conductivity–temperature curves of seven pairs of specimens in different rock groups.

Rock type and specimen no.	$A$ ( $10^{-6}$ )	$R^2$
Monzogranite (BS05-07)	8.821	0.9830
Granodiorite (BS06-05)	5.679	0.9334
Monzogranite (BS15-07)	8.394	0.9853
Granodiorite (BS16-05)	4.871	0.9289
Monzogranite (BS18-1-08)	6.891	0.9262
Granodiorite (BS18-2-05)	5.728	0.9581
Monzogranite (BS19-1-07)	6.385	0.9933

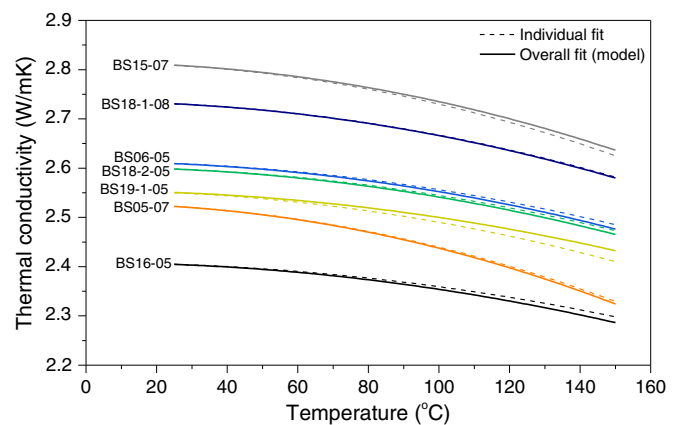


**Fig. 12.** Variation of the fit coefficient  $A$  of the thermal conductivity–temperature curves with rock porosity of seven pairs of specimens in different rock groups and its best fit.

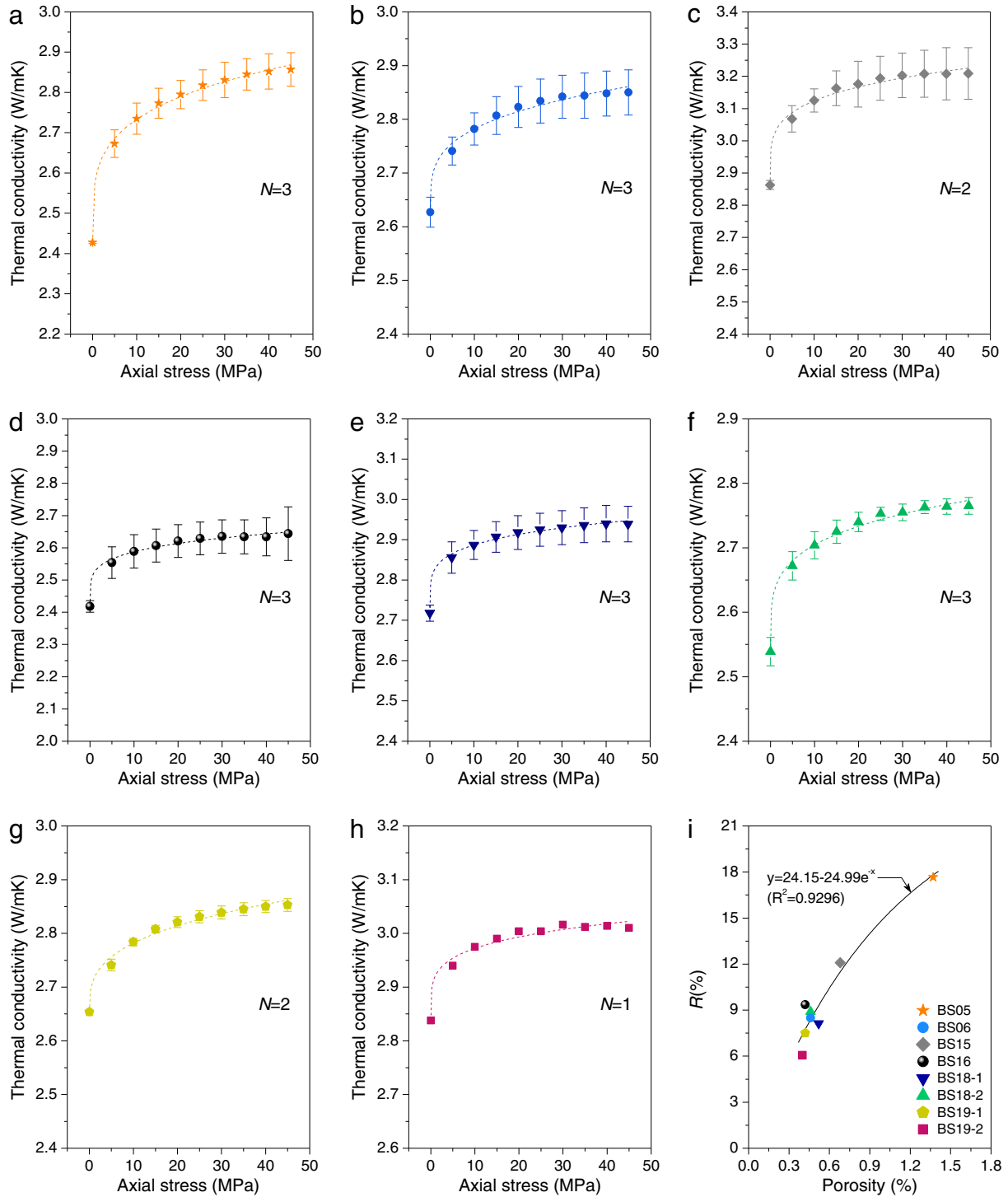
to 150 °C. The thermal conductivity of these specimens at room temperature (25 °C) was also measured and the data were added to this figure. It is seen that the thermal conductivity of the specimens shows a decaying trend with increasing temperature, and the values at 150 °C range from 5.7% to 8.7% lower than those at room temperature. This means that within the used temperature range, the influence of the increasing temperature on the decay of thermal conductivity for these rocks is limited. On the other hand, a possible reason for the gradual decrease in thermal conductivity is the generation of thermally induced microcracks in the rocks because of a mismatch between thermal expansion coefficients of adjacent mineral grains in a homogeneous temperature field (Jansen et al., 1993), which has been demonstrated from a microcracking perspective based on numerical simulations (Zhao, 2016). Based on the experimental data, the relationship between thermal conductivity and temperature can be described using the equation:

$$k = k_r - AT^2 \quad (8)$$

where  $k_r$  is the thermal conductivity of the rock at room temperature (25 °C),  $T$  is the temperature in Celsius, and  $A$  is the fit coefficient (see Table 3). The parameter  $A$  affects the decaying velocity of the thermal conductivity with the temperature, i.e., the decaying velocity of the thermal conductivity increases as  $A$  increases. As shown in Table 3,  $A$  in Eq. (8) varies from rock to rock and can be determined only using laboratory tests. In order to develop a model for predicting  $A$ ,



**Fig. 13.** Comparison of overall fit using the temperature and rock porosity dependent thermal conductivity model and individual fit of seven pairs of specimens in different rock groups.



**Fig. 14.** Influence of axial compression stress on the thermal conductivity of the eight rock groups: (a) BS05, (b) BS06, (c) BS15, (d) BS16, (e) BS18-1, (f) BS18-2, (g) BS19-1 and (h) BS19-2, and variation of the increase rate of the thermal conductivity ( $R$ ) with rock porosity (i). Error bars indicate the standard deviation of the thermal conductivity.  $N$  in the figures represents the number of specimen pairs in each rock group.

we attempted to relate  $A$  with other rock parameters and found that  $A$  depended on the magnitude of rock porosity ( $n$ ), as presented in Fig. 12. The coefficient  $A$  varies with porosity  $n$  according to the following equation:

$$A = 9.43 - 0.71/n^2 \quad (9)$$

According to Eqs. (8)–(9), an overall fit for different rock groups is made to illustrate the temperature dependent thermal

conductivity model considering rock porosity. Fig. 13 indicates that the results of the overall fit using the model agree well with the results of individual fit based on experimental data. It should be noted that the established Eqs. (8)–(9) are best-fit curves for thermal conductivity in range of test temperatures. Although they can be used to estimate the thermal conductivity within this range, they should not be extrapolated to temperatures lower than 25 °C or higher than 150 °C. On the other hand, the model was established by using limited data. When more test data are available, the model

**Table 4**

Fit coefficients for thermal conductivity-axial stress curves of Beishan granitic rocks under uniaxial compression.

Rock type and group	B	C	R <sup>2</sup>
Monzogranite (BS05)	0.174	0.244	0.9967
Granodiorite (BS06)	0.083	0.272	0.9869
Monzogranite (BS15)	0.158	0.218	0.9886
Granodiorite (BS16)	0.106	0.204	0.9909
Monzogranite (BS18-1)	0.106	0.203	0.9946
Granodiorite (BS18-2)	0.097	0.232	0.9929
Monzogranite (BS19-1)	0.061	0.323	0.9864
Monzogranite (BS19-2)	0.083	0.211	0.9780

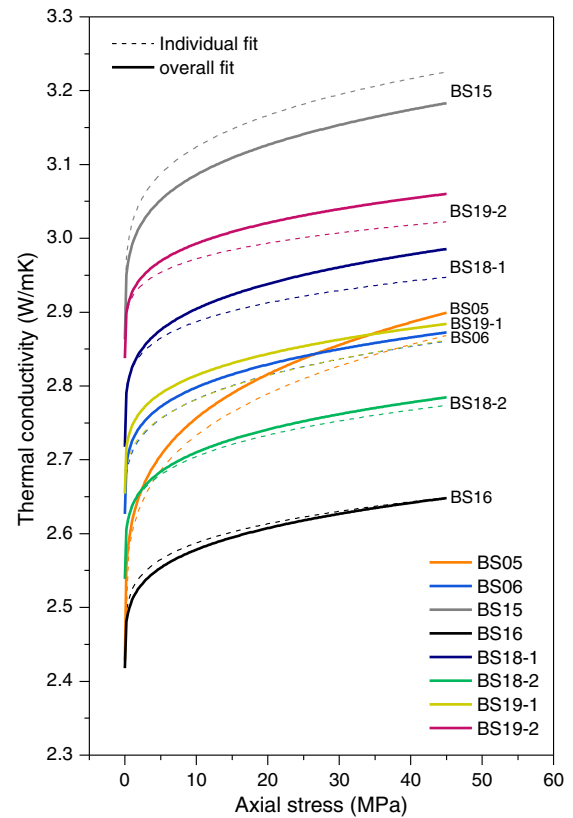
parameters can be fine-tuned to suit the temperature-dependent thermal conductivity of rocks.

#### 4.3. Influence of axial stress on the thermal conductivity

Under uniaxial compression condition, thermal conductivity measurements on 20 pairs of dry specimens in different rock groups were conducted. To analyze the thermal conductivity of the tested rocks with respect to axial stress, the experimental results were plotted on the graph as given in Fig. 14a–h. It can be observed that the thermal conductivities of all rocks vary with increasing axial stress in a nonlinear behavior, which is basically in agreement with the observations reported by other researchers (Clauser and Huenges, 1995; Demirci et al., 2004; Görgülü et al., 2008; Walsh and Decker, 1966). At the initial loading stage, there is a rapid increase of the thermal conductivities due to closure of pre-existing pores and microcracks in the rocks. In this stage, the increasing gradient of the thermal conductivities decreases as the axial stress increases. This means that the crack closure rate and axial stiffness of the rocks decreases and increases gradually, respectively. In the subsequent loading, the increasing gradient of the thermal conductivities changes little, which may represent that the elastic deformation of the rocks occurs. For each rock group, the increase rate ( $R$ ) of the thermal conductivity can be defined as:

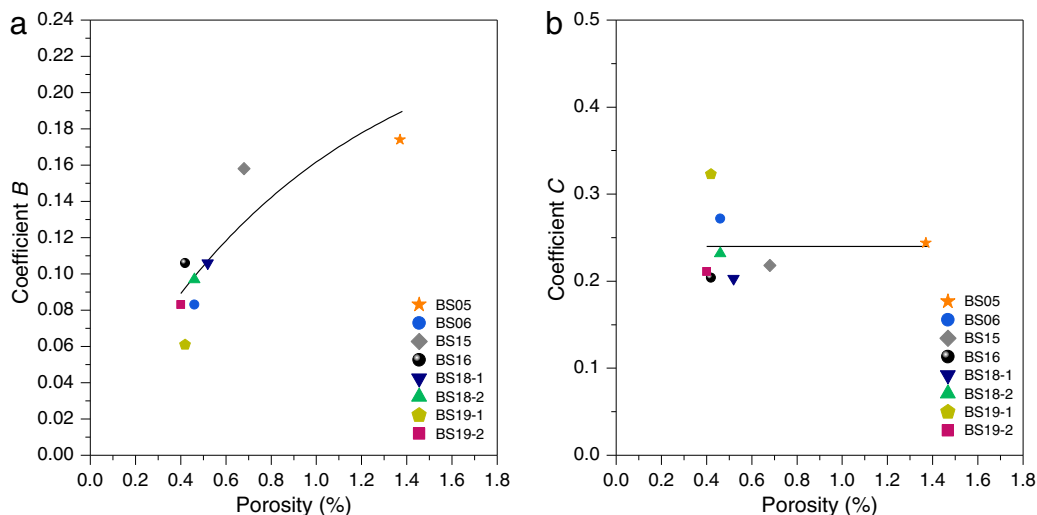
$$R = \frac{k_l - k_i}{k_i} \quad (10)$$

where  $k_l$  and  $k_i$  is the thermal conductivities of the specimens at the last compression stress level (i.e., 45 MPa) and before loading, respectively. The ratio  $R$  is found to be dependent on rock porosity, as shown in Fig. 14i. It is seen that  $R$  presents an increasing trend with increasing



**Fig. 16.** Comparison of overall fit using the axial stress and rock porosity dependent thermal conductivity model and individual fit of specimens in different rock groups.

porosity. For the tested rocks,  $R$  ranges from 6.1% to 17.7%. Inspection of Figs. 10 and 14i shows that the effects of compression stress and water saturation on the thermal conductivity are basically comparable. It should be mentioned that if the axial stress is further increased, new cracks in the rocks will be generated, propagated and coalesced. The stress-induced rock damage will result in deterioration of thermal conductivity (Chen et al., 2012). Hence, from low to high compression stress conditions, the thermal conductivity may increase to its peak value, after which it may decrease gradually. However, the influence of stress-induced damage on the thermal conductivity characteristics has been beyond the scope of this study. Based on the



**Fig. 15.** Variation of fit coefficients  $B$  (a) and  $C$  (b) of the thermal conductivity-axial stress curves with porosity of the eight rock groups.



currently obtained data, a best fitting equation of axial stress-dependent thermal conductivity for these rocks can be expressed as (Demirci et al., 2004)

$$k = k_0 + B\sigma_1^C \quad (11)$$

where  $k_0$  is the thermal conductivity of the rock at zero stress,  $\sigma_1$  is the axial stress, and  $B$  and  $C$  are fit coefficients, as listed in Table 4. Analysis of Eq. (11) reveals that the coefficient  $B$  plays a critical role in controlling the increasing gradient of the thermal conductivity in the initial loading stage (i.e., crack closure stage). The coefficient  $C$  dominantly affects the increasing velocity of the thermal conductivity in the subsequent elastic deformation stage. Based on experimental investigations on the thermal conductivity of some rocks subjected to uniaxial stresses using a steady-state apparatus developed by Demirci et al. (2004), Görgülü et al. (2008) found that the parameters  $B$  and  $C$  depended on the magnitude of elastic modulus of the rocks, and subsequently established an elastic modulus dependent model to predict the thermal conductivity values under pressure. Unfortunately, in the present study, the elastic moduli of the tested rocks have not been available. Therefore, the model proposed by Görgülü et al. (2008) cannot be used to fit our test results. According to Fig. 14, we found that the increasing gradients of the thermal conductivities in the initial loading stage were generally large for the rocks with a high porosity such as rock groups BS05 and BS15. Hence, the coefficient  $B$  is associated with the rock porosity  $n$ , i.e.,  $B$  increases as  $n$  increases, as presented in Fig. 15a. An exponential form expression can fit the data reasonably, as follows:

$$B = 0.25 - 0.24 \exp(-n) \quad (12)$$

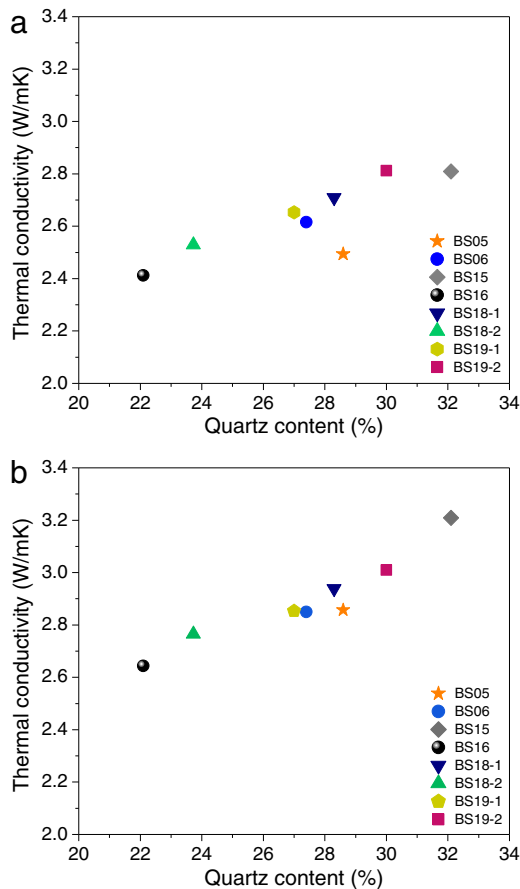


Fig. 17. Influence of quartz content on the average thermal conductivities of the eight rock groups in dry state (a) and compression state with an axial stress of 45 MPa (b).

Meanwhile, the coefficient  $C$  in Eq. (11) is not sensitive to the variation of rock porosity, and is within the range from 0.20 to 0.27 except for the rock group BS19-1. For simplicity, an average value of  $C = 0.24$  obtained from Table 4 is used to approximately describe the trend, as shown in Fig. 15b. Using Eqs. (11)–(12) and the constant coefficient  $C$ , an overall fit is made for these rock groups to reproduce the rock porosity-dependent thermal conductivity under different axial stresses. A comparison between individual and overall fit results is presented in Fig. 16. It is found that for each rock group subjected to different compression stresses, the difference of the thermal conductivity values from the individual and overall fits is less than 0.05 W/mK. The good agreement indicates that the established rock porosity-dependent model can capture the nonlinear stress-thermal conductivity relationships of the Beishan granitic rocks satisfactorily.

## 5. Discussion

One of the findings from the experimental investigations in the previous sections is that the rock porosity has an influence on the thermal conductivity of the Beishan granitic rocks under water saturation, increasing temperature and compression stress conditions, although the porosity of tested rocks is relatively low. It is well known that for low-porosity crystalline rocks, the mineral composition plays an important role in dominating the thermal conductivity. The crystalline rocks are mainly made up of quartz, feldspars, and mafic minerals such as pyroxene, amphibole and biotite, and the content of minerals from these three mineral groups basically determines a rock's thermal conductivity (Clauser and Huenges, 1995). As mentioned in Section 2, a model analysis on a total of 46 thin sections of the rocks was conducted to identify the dominant minerals in the rocks. As listed in Table 1, the main minerals of these rocks include quartz, plagioclase, K-feldspar and biotite. Among these four minerals, quartz has the highest thermal conductivity (7.69 W/mK) while another three minerals have a thermal conductivity range between 1.70 and 2.29 W/mK (Horai, 1971). Hence, when the porosity values of the specimens in different rock groups are close to each other, quartz content in the rocks may determine the thermal conductivity. According to the data listed in Table 2, Fig. 17a presents the influence of quartz content on the average thermal conductivity of different rock groups in dry state. It is seen that except for rock groups BS05 and BS15 (which have relatively large porosity values of 1.37% and 0.68%, respectively), thermal conductivity of the rocks appears an increasing trend with increasing quartz content. When the specimens are subjected to compression stresses, the original pores and cracks in the rocks tend to close, and the effective contact areas between mineral grains increase, leading to a significant decay of the porosity effect on the thermal conductivity, especially for rocks with relatively high porosity. On the other hand, the closure of pores and cracks increases the contact opportunity of quartz grains, and hence improves the transportation capability of heat flow in the rocks. Under this condition, an obvious increase of the thermal conductivity for all rock groups with increasing quartz content can be observed, as presented in Fig. 17b.

## 6. Conclusions

Beishan granitic rocks are candidate host rock types for China's HLW repository. In this paper, thermal conductivity characteristics of the Beishan granitic rocks have been investigated using the Transient Plane Source (TPS) method. The measurement results indicate that for the used eight rock groups with a porosity range from 0.40% to 1.37%, the average thermal conductivity values in the dry state range between 2.412 and 2.812 W/mK. The values under water-saturated condition range from 2.602 to 3.156 W/mK. Meanwhile, the effect of water saturation on thermal conductivity presents an increasing trend with an increase of rock porosity. Using several mixing models proposed by previous researchers, we found that the Hashin–Shtrikman mean model showed a reasonably good fit to the experimental data while another three models

(i.e., geometric mean, the arithmetic mean, and the effective-medium mean) yielded similar predictions and underestimated the thermal conductivity of the rocks under the water-saturated condition. Future work is demanded to verify the validity of various mixing models using different rock types with a large porosity range.

With increasing temperature from 25 °C to 150 °C, the thermal conductivity of the rocks shows a decaying trend and the values at 150 °C range from 5.7% to 8.7% lower than those at room temperature, revealing that the influence of temperature on the thermal conductivity of the tested rocks is limited. In addition, the thermal conductivity of the rocks increases with increasing compression stress in a nonlinear behavior, and the increase rate of the thermal conductivity increases with an increase of rock porosity. It is found that the effects of compression stress and water saturation on the magnitude of thermal conductivity of the rocks are basically comparable. Based on the experimental data, the empirical models considering the influence of rock porosity have been established for predicting the temperature and compression stress dependent thermal conductivity characteristics of the rocks, and the predictions are found to be in good agreement with experimental results. This study thus emphasizes importance of porosity on thermal conductivity measurements even for low porosity crystalline rocks.

When the pores and cracks in the rocks tend to close during compression, quartz content may determine the thermal conductivity, and there exists an increase of the thermal conductivity with increasing quartz content. This is because the closure of pores and cracks increases the contact opportunity of quartz grains, and hence improves the transportation capability of heat flow in the rocks. While the test results provide insights into the thermal conductivity characteristics of Beishan granitic rocks, one should be aware of the limitation of this study. Because the thermal conductivity of granitic rocks is influenced by many factors. In order to better understand the thermal conductivity of granitic rocks related to rock characteristics such as rock fabric, grain shape, grain contact and grain size, comprehensive petrographic investigations are recommended in the future. In the meantime, studies should be carried out to understand how the interactions between mineral components affect the thermal conductivity. Work is also being conducted to investigate the thermal conductivity of the rocks under coupled thermal-hydro-mechanical conditions.

## Acknowledgments

This work has been supported by the China Atomic Energy Authority through the geological disposal program and the National Natural Science Foundation of China (Grant no. 11102061). The authors also thank the two anonymous reviewers for their valuable comments and suggestions.

## References

- Abdulagatova, Z., Abdulagatov, I.M., Emirov, V.N., 2009. Effect of temperature and pressure on the thermal conductivity of sandstone. *Int. J. Rock Mech. Min. Sci.* 46, 1055–1071.
- Abdulagatova, Z., Abdulagatov, I.M., Emirov, S.N., 2010. Effect of pressure, temperature, and oil-saturation on the thermal conductivity of sandstone up to 250 MPa and 520 K. *J. Pet. Sci. Eng.* 73, 141–155.
- Adl-Zarrabi, B., 2004. Thermal Properties: Heat Conductivity and Heat Capacity Determined Using the TPS Method and Mineralogical Composition by Modal Analysis. *Svensk Kärnbränslehantering AB*.
- Alishaev, M.G., Abdulagatov, I.M., Abdulagatova, Z.Z., 2012. Effective thermal conductivity of fluid-saturated rocks: experiment and modeling. *Eng. Geol.* 135–136, 24–39.
- Barry-Macaulay, D., Bouazza, A., Singh, R.M., Wang, B., Ranjith, P.G., 2013. Thermal conductivity of soils and rocks from the Melbourne (Australia) region. *Eng. Geol.* 164, 131–138.
- Beck, A.E., Beck, J.M., 1958. On the measurement of the thermal conductivity of rocks by observations on a divided bar apparatus. *EOS Trans. Am. Geophys. Union* 30, 1111–1123.
- Birch, F., 1950. Flow of heat in the Front Range, Colorado. *Geol. Soc. Am. Bull.* 61, 567–630.
- Birch, F., Clark, H., 1940. The thermal conductivity of rocks and its dependence upon temperature and composition. *Am. J. Sci.* 238, 613–635.
- Brantberger, M., Zetterqvist, A., Arnbjerg-Nielsen, T., Olsson, T., Outters, N., Syrjänen, P., 2006. Final repository for spent nuclear fuel. Underground design Forsmark, Layout D1. SKB R-06-34. *Svensk kärnbränslehantering AB*.
- Bruggeman, D.A.G., 1935. Berechnung verschiedener Konstanten von heterogenen Substanzen – I. Dielektrizitätskonstanten und Leitfähigkeiten der Mischkörper aus isotropen Substanzen. *Ann. Phys.* 24, 636–679.
- Chen, Y.F., Li, D.Q., Jiang, Q.H., Zhou, C.B., 2012. Micromechanical analysis of anisotropic damage and its influence on effective thermal conductivity in brittle rocks. *Int. J. Rock Mech. Min. Sci.* 50, 102–116.
- Cho, W.-J., Kwon, S., 2010. Estimation of the thermal properties for partially saturated granite. *Eng. Geol.* 115, 132–138.
- Cho, W.J., Kwon, S., Choi, J.W., 2009. The thermal conductivity for granite with various water contents. *Eng. Geol.* 107, 167–171.
- Clauser, C., 2009. Heat transport processes in the Earth's crust. *Surv. Geophys.* 30, 163–191.
- Clauser, C., Huenges, E., 1995. Thermal conductivity of rocks and minerals. In: Ahrens, T.J. (Ed.), *Rock Physics and Phase Relations: A Handbook of Physical Constants*. American Geophysical Union, Washington, pp. 105–126.
- Demirci, A., Görgülü, K., Durutürk, Y.S., 2004. Thermal conductivity of rocks and its variation with uniaxial and triaxial stress. *Int. J. Rock Mech. Min. Sci.* 41, 1133–1138.
- Hot Disk, 2007. Instruction Manual of Hot Disk Thermal Constants Analyser Software Version 5.9. Hot Disk AB, Gothenburg.
- Fuchs, S., Schütz, F., Förster, H.-J., Förster, A., 2013. Evaluation of common mixing models for calculating bulk thermal conductivity of sedimentary rocks: correction charts and new conversion equations. *Geothermics* 47, 40–52.
- Görgülü, K., Durutürk, Y.S., Demirci, A., Poyraz, B., 2008. Influences of uniaxial stress and moisture content on the thermal conductivity of rocks. *Int. J. Rock Mech. Min. Sci.* 45, 1439–1445.
- Gustafsson, S.E., 1991. Transient plane source techniques for thermal conductivity and thermal diffusivity measurements of solid materials. *Rev. Sci. Instrum.* 62, 797–804.
- Hartmann, A., Rath, V., Clauser, C., 2005. Thermal conductivity from core and well log data. *Int. J. Rock Mech. Min. Sci.* 42, 1042–1055.
- Hashin, Z., Shtrikman, S., 1962. A variational approach to the theory of the effective magnetic permeability of multiphase materials. *J. Appl. Phys.* 33, 3125–3131.
- Heuze, F.E., 1983. High-temperature mechanical, physical and thermal properties of granitic rocks – a review. *Int. J. Rock Mech. Min. Sci. Geomech. Abstr.* 20, 3–10.
- Hökmak, H., Lönnqvist, M., Kristensson, O., Sundberg, J., Hellström, G., 2009. Strategy for thermal dimensioning of the final repository for spent nuclear fuel. SKB R-09-04. *Svensk kärnbränslehantering AB*.
- Horai, K., 1971. Thermal conductivity of rock-forming minerals. *J. Geophys. Res.* 76, 1278–1308.
- Hudson, J.A., Cosgrove, J.W., Kemppainen, K., Johansson, E., 2011. Faults in crystalline rock and the estimation of their mechanical properties at the Olkiluoto site, western Finland. *Eng. Geol.* 117, 246–258.
- Jackson, R.D., Taylor, S.A., 1986. Thermal conductivity and diffusivity. *Methods of Soil Analysis, Part 1. Physical and Mineralogical Methods*, pp. 945–956.
- Jansen, D.P., Carlson, S.R., Young, R.P., Hutchins, D.A., 1993. Ultrasonic imaging and acoustic emission monitoring of thermally induced microcracks in Lac du Bonnet granite. *J. Geophys. Res.* 98, 22231–22243.
- Lagtiela, S., Bison, P., Peron, F., Romagnoni, P., 2015. Thermal conductivity measurements on wood materials with transient plane source technique. *Thermochim. Acta* 600, 45–51.
- Lichtenecker, K., 1924. Der elektrische Leitungswiderstand kunstlicher und natürlicher Aggregate. *Phys. Z.* 25 (pp. 169–181, 193–204, 226–233).
- Log, T., Gustafsson, S.E., 1995. Transient plane source (TPS) technique for measuring thermal transport properties of building materials. *Fire Mater.* 19, 43–49.
- Miao, S.Q., Li, H.P., Chen, G., 2014. Temperature dependence of thermal diffusivity, specific heat capacity, and thermal conductivity for several types of rocks. *J. Therm. Anal. Calorim.* 115, 1057–1063.
- Mottaghy, D., Vosteen, H.D., Schellschmidt, R., 2008. Temperature dependence of the relationship of thermal diffusivity versus thermal conductivity for crystalline rocks. *Int. J. Earth Sci.* 97, 435–442.
- Nagaraju, P., Roy, S., 2014. Effect of water saturation on rock thermal conductivity measurements. *Tectonophysics* 626, 137–143.
- Özkahraman, H.T., Selver, R., Isik, E.C., 2004. Determination of the thermal conductivity of rock from P-wave velocity. *Int. J. Rock Mech. Min. Sci.* 41, 703–708.
- Pasquale, V., Cosdoya, M., Chiozzi, P., 2015. Measurements of rock thermal conductivity with a Transient Divided Bar. *Geothermics* 53, 183–189.
- Popov, Y.A., Pribnow, D.F.C., Sass, J.H., Williams, C.F., Burkhardt, H., 1999. Characterization of rock thermal conductivity by high-resolution optical scanning. *Geothermics* 28, 253–276.
- Popov, Y., Tertychnyi, V., Romushkevich, R., Korobkov, D., Pohl, J., 2003. Interrelations between thermal conductivity and other physical properties of rocks: experimental data. *Pure Appl. Geophys.* 160, 1137–1161.
- Ray, L., Bhattacharya, A., Roy, S., 2007. Thermal conductivity of Higher Himalayan Crystallines from Garhwal Himalaya, India. *Tectonophysics* 434, 71–79.
- Ray, L., Förster, H.-J., Förster, A., Fuchs, S., Naumann, R., Appelt, O., 2015. Tracking the thermal properties of the lower continental crust: measured versus calculated thermal conductivity of high-grade metamorphic rocks (Southern Granulite Province, India). *Geothermics* 55, 138–149.
- Sass, J.H., Lachenbruch, A.H., Munroe, R., 1971. Thermal conductivity of rocks from measurements on fragments and its application to heat flow determinations. *J. Geophys. Res.* 76, 2291–3401.
- Sibbitt, W.L., 1976. Preliminary Measurements of the Thermal Conductivity of Rocks from LASL Geothermal Test Holes GT-1 and GT-2. Los Alamos scientific laboratory of the University of California, pp. 1–8.

- Solórzano, E., Reglero, J.A., Rodríguez-Pérez, M.A., Lehmann, D., Wichmann, M., de Saja, J.A., 2008. An experimental study on the thermal conductivity of aluminium foams by using the transient plane source method. *Int. J. Heat Mass Transf.* 51, 6259–6267.
- Streckeisen, A.L., 1976. To each plutonic rock its proper name. *Earth Sci. Rev.* 12, 1–33.
- Sundberg, J., Hellström, G., 2009. Inverse modelling of thermal conductivity from temperature measurements at the Prototype Repository, Äspö HRL. *Int. J. Rock Mech. Min. Sci.* 46, 1029–1041.
- Sundberg, J., Wrafter, J., Back, P.-E., Rosén, L., 2008. Thermal properties Laxemar. Site descriptive modelling SDM-Site Laxemar. SKB R-08-61. Svensk kärnbränslehantering AB.
- Sundberg, J., Back, P.-E., Ericsson, L.O., Wrafter, J., 2009. Estimation of thermal conductivity and its spatial variability in igneous rocks from *in situ* density logging. *Int. J. Rock Mech. Min. Sci.* 46, 1023–1028.
- Urquhart, A., Bauer, S., 2015. Experimental determination of single-crystal halite thermal conductivity, diffusivity and specific heat from  $-75^{\circ}\text{C}$  to  $300^{\circ}\text{C}$ . *Int. J. Rock Mech. Min. Sci.* 78, 350–352.
- Voigt, W., 1928. *Lehrbuch der Kristallphysik*. Teubner, p. 978 (Leipzig).
- Von Herzen, R.P., Maxwell, A.E., 1959. The measurement of thermal conductivity of deep-sea sediments by a needle probe method. *J. Geophys. Res.* 64, 1557–1563.
- Vosteen, H.D., Schellschmidt, R., 2003. Influence of temperature on thermal conductivity, thermal capacity and thermal diffusivity for different types of rock. *Phys. Chem. Earth* 28, 499–509.
- Walsh, J.B., Decker, E.R., 1966. Effect of pressure and saturating fluid on the thermal conductivity of compact rock. *J. Geophys. Res.* 71, 3053–3061.
- Wang, J., 2010. High-level radioactive waste disposal in China: update 2010. *J. Rock Mech. Geotech. Eng.* 2, 1–11.
- Wang, J., 2014. On area-specific underground research laboratory for geological disposal of high-level radioactive waste in China. *J. Rock Mech. Geotech. Eng.* 6, 99–104.
- Xu, G., LaManna, J.M., Clement, J.T., Mench, M.M., 2014. Direct measurement of through-plane thermal conductivity of partially saturated fuel cell diffusion media. *J. Power Sources* 256, 212–219.
- Yang, Y.X., Voskuilen, T.G., Pourpoint, T.L., Guildenbecher, D.R., Gore, J.P., 2012. Determination of the thermal transport properties of ammonia borane and its thermolysis product (polyiminoborane) using the transient plane source technique. *Int. J. Hydrog. Energy* 37, 5128–5136.
- Zhao, Z.H., 2016. Thermal influence on mechanical properties of granite: a microcracking perspective. *Rock Mech. Rock. Eng.* 49, 747–762.
- Zhao, X.G., Wang, J., Cai, M., Ma, L.K., Zong, Z.H., Wang, X.Y., Su, R., Chen, W.M., Zhao, H.G., Chen, Q.C., An, Q.M., Qin, X.H., Ou, M.Y., Zhao, J.S., 2013. In-situ stress measurements and regional stress field assessment of the Beishan area, China. *Eng. Geol.* 163, 26–40.
- Zhao, X.G., Cai, M., Wang, J., Li, P.F., 2015a. Strength comparison between cylindrical and prism specimens of Beishan granite under uniaxial compression. *Int. J. Rock Mech. Min. Sci.* 76, 10–17.
- Zhao, X.G., Cai, M., Wang, J., Li, P.F., Ma, L.K., 2015b. Objective determination of crack initiation stress of brittle rocks under compression using AE measurement. *Rock Mech. Rock. Eng.* 48, 2473–2484.
- Zimmerman, R.W., 1989. Thermal conductivity of fluid-saturated rocks. *J. Pet. Sci. Eng.* 3, 219–227.